



Sliding Relations for Glacier Slip With Cavities Over Three-Dimensional Beds

Christian Helanow, Neal R. Iverson, Lucas K. Zoet, Olivier Gagliardini

► To cite this version:

Christian Helanow, Neal R. Iverson, Lucas K. Zoet, Olivier Gagliardini. Sliding Relations for Glacier Slip With Cavities Over Three-Dimensional Beds. *Geophysical Research Letters*, 2020, 47, 10.1029/2019GL084924 . insu-03706476

HAL Id: insu-03706476

<https://insu.hal.science/insu-03706476>

Submitted on 28 Jun 2022

HAL is a multi-disciplinary open access archive for the deposit and dissemination of scientific research documents, whether they are published or not. The documents may come from teaching and research institutions in France or abroad, or from public or private research centers.

Copyright

L'archive ouverte pluridisciplinaire **HAL**, est destinée au dépôt et à la diffusion de documents scientifiques de niveau recherche, publiés ou non, émanant des établissements d'enseignement et de recherche français ou étrangers, des laboratoires publics ou privés.

Geophysical Research Letters

RESEARCH ARTICLE

10.1029/2019GL084924

Key Points:

- Drag at rigid glacier beds during basal slip with ice-bed separation depends sensitively on the three-dimensional bedrock morphology
- Lateral spacing of bed obstacles affects the degree of rate-weakening drag, in which drag decreases with increasing slip velocity
- Bed obstacles with steep adverse slopes stabilize slip by causing drag to increase over a wide range of increasing slip velocity

Supporting Information:

- Supporting Information S1

Correspondence to:

C. Helanow,
helanow@iastate.edu

Citation:

Helanow, C., Iverson, N. R., Zoet, L. K., & Gagliardini, O. (2020). Sliding relations for glacier slip with cavities over three-dimensional beds. *Geophysical Research Letters*, 47, e2019GL084924. <https://doi.org/10.1029/2019GL084924>

Received 9 AUG 2019

Accepted 3 DEC 2019

Accepted article online 17 DEC 2019

Sliding Relations for Glacier Slip With Cavities Over Three-Dimensional Beds

Christian Helanow¹, Neal R. Iverson¹, Lucas K. Zoet², and Olivier Gagliardini³

¹Department of Geological and Atmospheric Sciences, Iowa State University, Ames, IA, USA, ²Department of Geoscience, University of Wisconsin-Madison, Madison, WI, USA, ³Univ. Grenoble Alpes, CNRS, IRD, IGE, Grenoble, France

Abstract Results of glacier flow models and associated estimates of future sea level rise depend sensitively on the prescribed relation between shear stress and slip velocity at the glacier bed. Using a fully three-dimensional numerical model of ice flow, we compute steady-state sliding relations for where ice slips over a rock bed with three-dimensional, periodic topography. In agreement with studies of two-dimensional beds, water-filled cavities that form down-glacier from bedforms cause basal shear stress to peak at a threshold slip velocity and decrease at higher velocities (i.e., rate-weakening drag). However, the shear stress magnitude and extent of rate-weakening drag depend systematically on lateral topographic variations not considered previously. Moreover, steep up-glacier-facing slopes of bedforms can result in shear stress that increases monotonically over a wide range of slip velocity, helping to stabilize slip. These results highlight the potential variability of sliding relations and their likely sensitivity to the morphological diversity of glacier beds.

Plain Language Summary Parts of ice sheets that flow into the oceans and affect sea level can flow unusually fast by slipping over their beds. We use a computer to solve for the first time in three dimensions the equations that describe the flow of ice as it slips over a bumpy rock bed. We include the important tendency for glaciers to separate from rock and form water-filled cavities down-glacier from bumps. These calculations indicate that resistance to slip depends sensitively on the bump shape and spacing. Cavities can cause the bed to become more slippery the faster the ice slides, with this destabilizing effect being more severe for bumps that are laterally narrow and widely spaced. However, bumps with steeply sloping up-glacier sides can reverse this effect and cause resistance to slip to increase over a wide range of increasing slip velocity. This diverse behavior highlights the need for estimates of glacier slip velocity to incorporate the actual topography of glacier beds.

1. Introduction

Ice sheets and smaller glaciers rest directly on beds consisting of rigid rock (hard bed) or deformable sediment (soft bed). In either case, glaciers move primarily by slip over their beds if basal ice is at the melting temperature (Cuffey & Paterson, 2010; Maier et al., 2019). Slip of ice over hard beds has diverse consequences. Over periods of up to a few years, some glaciers with hard beds can surge (i.e., increase their speeds commonly by a factor of 10–100) (Kamb, 1987; Thøgersen et al., 2019), causing rapid glacier advance and severe local environmental change (Harrison et al., 2015). Moreover, although large sections of fast-flowing Antarctic ice streams rest on soft beds, recent geophysical studies of the largest West Antarctic ice stream, Thwaites Glacier, indicate that parts of it are hard-bedded (Muto et al., 2019) and drag from slip across hard-bedded regions is higher than where the bed is soft (Koellner et al., 2019). Therefore, at Thwaites Glacier and potentially other ice streams in Antarctica and Greenland, slip where ice is in direct contact with rock could disproportionately affect ice-stream speed and associated sea level rise (Koellner et al., 2019). Also, hard beds are subject to erosion by glaciers at rates that depend directly on slip velocity (Hallet, 1979, 1996; Hooyer et al., 2012). This erosion, over timescales of 10^4 – 10^6 years, results in Alpine landscapes emblematic of glaciation, such as U-shaped and hanging valleys. It also results in denudation that modulates uplift of mountain belts (e.g., Pelletier, 2008) and alters climate through effects on chemical weathering rates (e.g., Torres et al., 2017). Thus, efforts to model both glacier flow (e.g., Bindschadler et al., 2013; Ritz et al., 2015) and glacial landscape evolution (e.g., Egholm et al., 2009; Herman et al., 2011; Pedersen & Egholm, 2013) require accurate descriptions of basal slip on hard beds.

Most commonly in numerical ice sheet models, slip at the bed is prescribed as a boundary condition, by relating the basal shear stress, τ_b , to the basal slip velocity, u_b , through a relation of the form

$$u_b = \beta \tau_b^q, \quad (1)$$

where q is a positive constant. In this slip relation the conditions at the bed (e.g., local bedrock topography, subglacial hydrology, and sediment characteristics) are combined in the static, spatially varying parameter β , which can be determined by inverse modeling using surface velocity observations (e.g., Brinkerhoff & Johnson, 2013; Gillet-Chaulet et al., 2016; Larour et al., 2012; Morlighem et al., 2010). This empirical parameter, however, and the form of the relation are main sources of uncertainty for prognostic simulations (Bindschadler et al., 2013; Brondex et al., 2017; Joughin et al., 2019; Ritz et al., 2015). In efforts to better include the well-documented influence of effective pressure N (defined as the ice pressure minus basal water pressure, $p_i - p_w$) on slip velocity (e.g., Iken & Bindschadler, 1986; Jansson, 1995), several contrasting modifications to equation (1) have been proposed (Budd et al., 1979; Schoof, 2005; Tsai et al., 2015). Numerical ice-flow models (e.g., Brondex et al., 2017) indicate that ice fluxes can be highly sensitive to these modifications; sensitivity of bedrock erosion rates to the form of the slip relation of landscape evolution models is only beginning to be explored (Ugelvig & Egholm, 2018).

Process-based theories of glacier sliding over hard, wavy, two-dimensional (2-D) beds (e.g., Fowler, 1981; Gudmundsson, 1997; Kamb, 1970; Lliboutry, 1968; Nye, 1969; Weertman, 1957) indicate that, in the absence of cavity formation downstream from the leesides of rock bumps, an appropriate sliding relation is of the form equation (1). Such cavities, however, are ubiquitous on hard glacier beds (Hallet & Anderson, 1980; Walder & Hallet, 1979). Iken (1981) showed that for 2-D periodic bumps with cavities there must be an upper bound on the drag exerted by the bed on the ice. As N decreases (p_w in cavities increases) and cavities grow, τ_b/N is bounded by the maximum value of the up-glacier-facing (stoss) slopes of obstacles, m_{\max} . This limit on basal drag is called Iken's bound:

$$\tau_b/N \leq m_{\max}. \quad (2)$$

It is in contrast to the unbounded basal shear stress of equation (1). Schoof (2005) showed that Iken's bound holds for arbitrary 2-D bed geometries, in agreement with earlier studies of slip over 2-D sinusoidal beds (Fowler, 1986, 1987; Lliboutry, 1968).

Furthermore, sliding theories that include cavities (Fowler, 1986, 1987; Gagliardini et al., 2007; Lliboutry, 1968; Schoof, 2005) indicate that drag reaches a local maximum, after which a further increase in u_b or decrease in N results in decreasing drag. We call this rate-weakening drag, and it results from cavity growth with increasing sliding velocity that restricts diminishing zones of ice-bed contact to near bump crests. Thus, on convex bumps these zones are inclined up-glacier at progressively smaller angles, thereby reducing drag. Experiments with 2-D periodic bumps demonstrate that rate-weakening drag can occur over a wide range of sliding velocities (Zoet & Iverson, 2015, 2016). The implications of the bed effectively becoming slippery with increasing u_b (or decreasing N) is that reduced shear stresses on the glacier bed would focus stresses elsewhere, promoting still faster glacier flow. To date, however, theoretical and experimental studies of glacier sliding relations with cavity formation have been restricted to only 2-D (transverse) bedforms, leaving the relevance of rate-weakening drag to real glacier beds uncertain. Large-scale glacier flow models universally neglect the potential for rate-weakening drag.

Herein we present the first computations of sliding relations for three-dimensional (3-D) hard beds with cavity formation. Using a fully 3-D numerical model of ice flow, we show that adding bed topography in a direction perpendicular to the slip direction can significantly enhance rate weakening. Importantly, however, we demonstrate for the first time that bumps with sufficiently steep up-glacier-facing slopes can eliminate this rate weakening over a wide range of potential slip velocity. These results, therefore, point to how the cavities of hard glacier beds may not necessarily preclude the rate-strengthening slip relations of glacier flow models.

2. Methods

We follow the general method and assumptions of Gagliardini et al. (2007), extending their formulation from 2-D to 3-D flow. Ice is assumed to be at the melting point (isothermal), resulting in a thin water film at the

ice-bed interface (e.g., Weertman, 1957). The large difference between the viscosity of ice and water leads to zero tangential stress, σ_{nt} , supported locally at both the bed surface (free slip) and ice-cavity boundary. Furthermore, we consider water pressure at the bed to be uniform and neglect regelation and basal melting. The underlying bed, z_b , is considered to be rigid and impenetrable, providing a surface beneath which the sole of the glacier, z_s , cannot move. If the water pressure is larger than the ice normal stress on the underlying bed, the ice separates from the bed forming a cavity. At the ice-cavity interface, the water pressure sets the normal stress, and z_s evolves as a free surface until a steady geometry is reached. These assumptions are in line with those made previously when considering glacier sliding over hard beds (e.g., Fowler, 1987; Gagliardini et al., 2007; Lliboutry, 1968; Schoof, 2005).

To avoid simulating flow across the full glacier thickness, the domain is vertically restricted to a boundary layer (Fowler, 1981; Gagliardini et al., 2007; Schoof, 2005) much thicker than the sizes of obstacles on the bed. At the top of the domain a horizontal speed, u_e , and vertical stress (ice pressure), p_i , are specified, with the vertical velocity left free to vary spatially. The vertical stress condition approximates the stress caused by the overlying column of ice due to gravity, which can be neglected in the boundary layer, whereas the horizontal velocity represents the bulk flow outside of the domain. Specifying a velocity rather than a shear stress is necessary to achieve flow regimes in which rate-weakening drag can occur and is also more appropriate when simulating the local effects of sliding. At the sides of the domain, the flow is periodic.

The above scenario is described by the Stokes (balance of momentum and mass) and kinematic free-surface equations (see Text S1 in the supporting information), where the primary assumptions are reflected in the boundary conditions. If we let z_s be subdivided into nonoverlapping parts where the glacier sole is in contact with the bed (z_{con} , i.e., where $z_s = z_b$) and where it is a part of the cavity roof (z_{cav} , i.e., where $z_s > z_b$), and let σ and σ_{nn} denote the Cauchy stress tensor and the normal stress at the boundary, the system of equations describing the problem are as follows:

$$\nabla \cdot \sigma = \mathbf{0} \quad (\text{momentum}), \quad (3a)$$

$$\nabla \cdot \mathbf{u} = 0 \quad (\text{incompressibility}), \quad (3b)$$

$$\sigma_{nn} = -p_i, \quad u_x = u_e, \quad u_y = 0 \quad (\text{top boundary}), \quad (3c)$$

$$\sigma_{nt} = 0 \quad \text{on } z_s \quad (\text{free slip}), \quad (3d)$$

$$\mathbf{u} \cdot \mathbf{n} = 0 \quad \text{on } z_{con} \quad (\text{impenetrability}), \quad (3e)$$

$$\sigma_{nn} = -p_w \quad \text{on } z_{cav} \quad (\text{cavity roof}), \quad (3f)$$

$$|\sigma_{nn}| \geq p_w \quad \text{on } z_s \quad (\text{ice-bed contact}), \quad (3g)$$

$$\partial_t z_s + u_x \partial_x z_s + u_y \partial_y z_s = u_z \quad (\text{free surface}), \quad (3h)$$

$$z_s \geq z_b \quad (\text{bed constraint}), \quad (3i)$$

where \mathbf{n} is the normal pointing outward from the domain and $\mathbf{u} = (u_x, u_y, u_z)$ is the velocity. A steady geometry is reached when the glacier sole has evolved to be such that $\mathbf{u} \cdot \mathbf{n} = 0$ everywhere on z_s . The constitutive equation for ice deformation relates the effective shear stress τ_E , to the effective strain rate, $\dot{\epsilon}_E$, as

$$\tau_E = B \dot{\epsilon}_E^{1/n}, \quad (4)$$

where the creep exponent $n = 3$ for ice (Glen, 1955). The rate factor B depends on temperature (Hooke, 2005) but in this case is uniform for ice at its pressure-melting temperature.

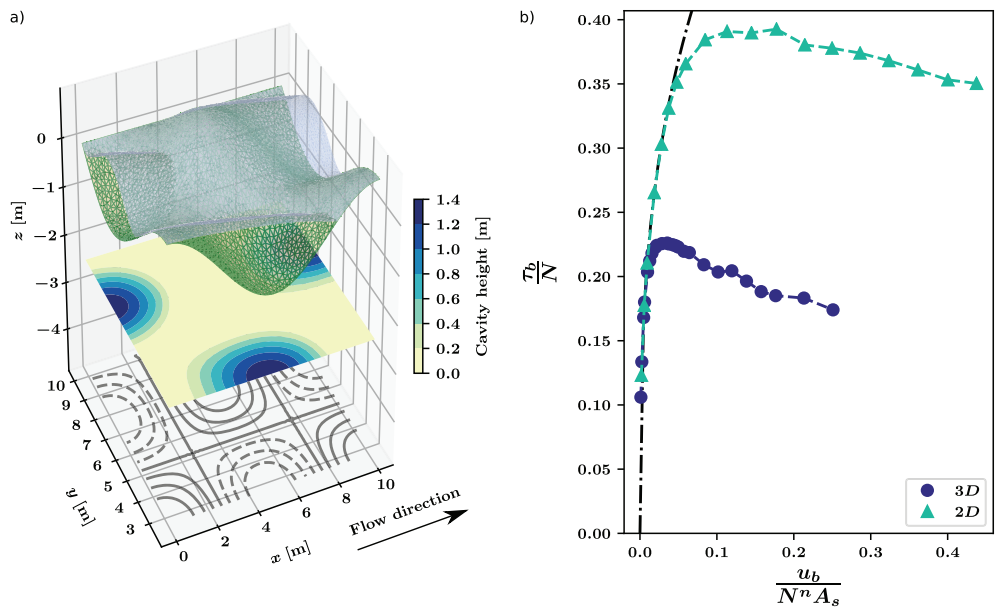


Figure 1. Modeling results for the cross-sinusoidal bed. (a) Bed geometry and steady-state cavity configuration with $u_b = 27.0$ m/year and $N = 0.4$ MPa. The top layer shows the glacier sole (light blue and transparent) with the underlying bed in green. The middle layer shows color-coded contours of the cavity height (vertical distance from glacier sole to bed). Elevation contours of the bed are shown at the bottom (solid black for positive elevations and dashed black for negative, with a contour interval of 0.2 m). The cross-section through one of the cavities is at $y = 2.5$ m. (b) Sliding relation for the cross-sinusoidal bed (blue circles) and for sliding without cavitation (equation (8), dash-dotted black line). Also shown are the results for the bed that is sinusoidal in only the along-flow direction (green triangles). The scaled range of calculated sliding velocity corresponds to dimensional values of $u_b = 0.3\text{--}66.8$ m/year for $N = 0.4$ MPa. For both relations a range of boundary condition velocities of 0.5–70 m/year was used.

For a given bed geometry, τ_b is the average drag due to viscous flow calculated along the glacier flow direction, x (e.g., Fowler, 1987; Lliboutry, 1968; Schoof, 2005):

$$\tau_b = -\frac{1}{\Omega} \int_{z_s} \sigma_{nn} n_x \, ds = -\frac{1}{\Omega} \int_{z_s} \sigma_{nn} \frac{\partial z_s}{\partial x} \, dx \, dy, \quad (5)$$

where Ω is the area of the domain in the horizontal plane and the integral results in a negative (up-glacier) value. Similarly, the average slip velocity in the direction of glacier flow is given by

$$u_b = \frac{1}{\Omega} \int_{z_s} u_x \, dx \, dy, \quad (6)$$

extending to 3-D the relations used in Gagliardini et al. (2007).

To solve the problem numerically, we use the finite element software Elmer/Ice (Gagliardini et al., 2013), which is a glacier-focused extension of the finite element code Elmer (Lyly et al., 1999; Råback et al., 2019), used by Gagliardini et al. (2007). All flow simulations are performed on meshes resulting from a triangulated horizontal base mesh that has been extruded in 20 layers in the vertical direction, giving prismatic/wedge elements. The vertical extrusion is the same for all simulations in this study, with the vertical mesh density approximately 10 times greater close to the bed than at the top of the domain. All of the base meshes were generated using Gmsh (Geuzaine & Remacle, 2009) and are unstructured on a 10-m \times 10-m grid consisting of 6,664 triangles, resulting in 133,280 elements (see Text S1 for additional information).

3. Results

To be able to compare the sliding relations for different scenarios, we present the relations in scaled, nondimensional form (Fowler, 1986; Gagliardini et al., 2007; Schoof, 2005), as drag relations:

$$\tau_b/N = f \left(\frac{u_b}{N^n A_s} \right), \quad (7)$$

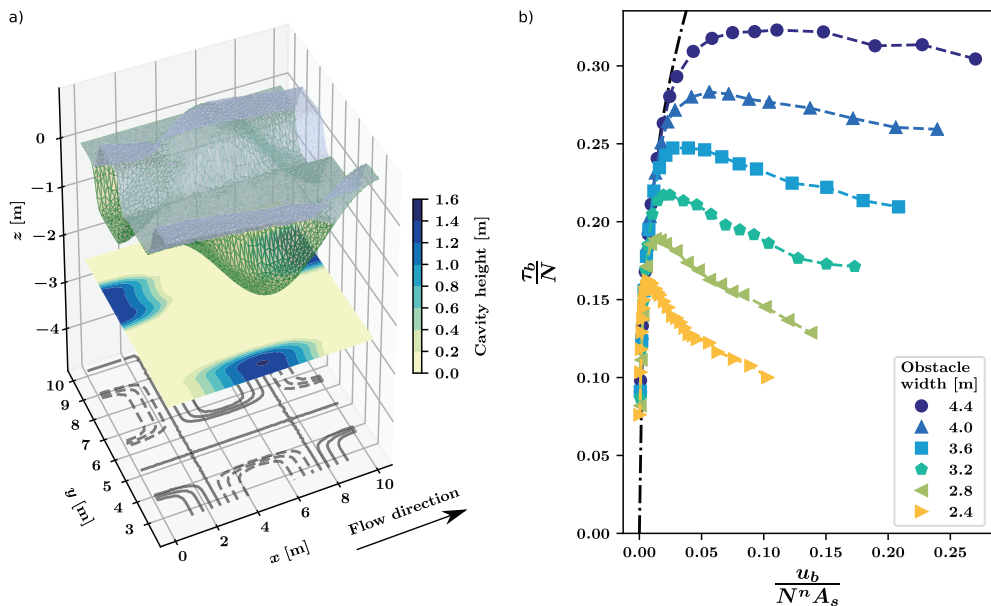


Figure 2. Modeling results for obstacles with different widths and spacings. (a) Bed geometry and steady-state cavity configuration for along-flow sinusoidal obstacles of width $w = 2.4$ m, with $u_b = 13.0$ m/year and $N = 0.4$ MPa. Otherwise, same as Figure 1a. (b) Sliding relations for along-flow sinusoidal obstacles of varying width. Smaller widths correspond to larger spacings of obstacles.

where τ_b/N has the form of a friction coefficient. The constant A_s depends on the bed geometry and B^{-n} (equation (4)) (e.g., Fowler, 1981; Gagliardini et al., 2007; Gudmundsson, 1997; Lliboutry, 1968) and relates τ_b and u_b for sliding without cavities:

$$u_b = A_s \tau_b^n. \quad (8)$$

Hence, using the scaled variables in equation (7) should, in principle, result in a relation $\tau_b/N \propto u_b^{1/n}/N$ at low sliding velocities before the onset of cavitation. Once cavities are initiated, equation (8) becomes invalid, and the increasingly large cavities can result in either rate-strengthening (f in equation (7) increases monotonically) or rate-weakening (f decreases after reaching an initial local maximum) drag. For the boundary conditions in equations (3c) and (3f), we apply $p_i = 2.0$ MPa and $p_w = 1.6$ MPa ($N = 0.4$ MPa) for all simulations. This is equivalent to approximately 200 m of ice overlying the domain, with water pressure in cavities being 80% of the overburden pressure. The height of the domain is set to 10 m.

To determine a sliding relation for a specified bed geometry, we consider a wide range of steady velocities at the domains top, u_e in equation (3c). Using simulation results at low speeds with no cavitation, the value of A_s is calculated using equation (8), and for each additional value of velocity at the domain's top, the roof of the cavity is allowed to evolve until a steady geometry is reached, at which point τ_b and u_b are numerically calculated using equations (5) and (6).

Before applying the model to fully 3-D bed geometries, we verified that it reproduces the results obtained in Gagliardini et al. (2007) for a sinusoidal bed by considering an extension of their 2-D domain with no roughness in the added transverse dimension (Figure S1).

To verify that the form of the sliding relation is not sensitive to the scaling procedure or computational domain, we for the bed studied in section 3.1 performed simulations in which the effective pressure, N , rather than the imposed horizontal velocity at the top boundary, was varied (Figure S2). Additionally, simulations were conducted using a greater domain height (20 m vs. 10 m) and a different mesh resolution. None of these changes affected significantly the results, implying that the scaling used in equation (7) is suitable and that the overall form of the relation is not sensitive to the domain parameters.

3.1. Cross-Sinusoidal Bed

We begin by examining how the sliding relation is affected by 3-D bed topography of the form

$$z_b(x, y) = 0.8 \cos(2\pi x/10) \sin(2\pi y/10) \quad 0 \leq x, y \leq 10$$

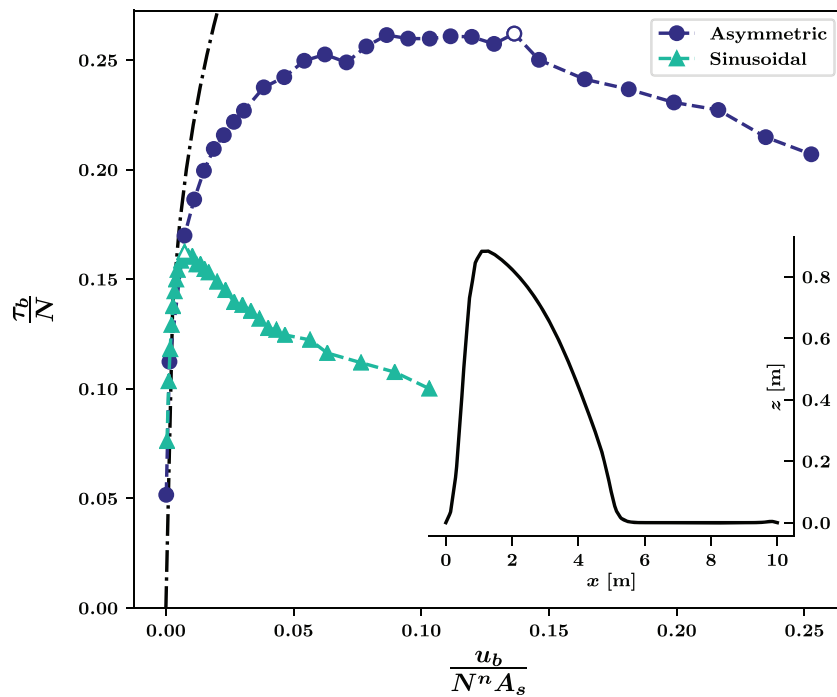


Figure 3. Sliding relation for asymmetric obstacles with steep stoss surfaces and width, $w = 2.4$ m. The inset shows an along-flow profile across one of the obstacles, with the direction of flow from left to right. Also shown, for comparison, are results from an otherwise identical bed but with obstacles that have sinusoidal along-flow profiles (the sliding relation for $w = 2.4$ m in Figure 2b). The scaled slip velocity corresponds to dimensional values of $u_b = 0.1\text{--}143$ m/year, and the peak drag $\tau_b/N = 0.26$ occurs at $u_b = 77.2$ m/year (blue and white circle). For the along-flow sinusoidal profile, the peak drag occurs at $u_b = 2.2$ m/year (green and white triangle).

(Figure 1a). Such a cross-sinusoidal bed is the simplest extension of the 2-D sinusoids used in previous studies (e.g., Fowler, 1986; Lliboutry, 1968; Nye, 1969). For small values of u_b , there are no cavities, and drag increases with slip velocity according to equation (8) (Figure 1b). At velocities where slip relations for ice flow with and without cavities bifurcate, cavities initiate. At a higher velocity, the drag peaks and then decreases at still higher velocities as cavities extend across most of stoss surfaces (Figure 1a). The rate of postpeak decline in drag with slip velocity (rate weakening) is similar for the cross-sinusoidal bed and for the analogous 2-D bed. More pronounced is the difference in magnitudes of the peak basal drags: The three-dimensionality of the bed reduces τ_b/N by 43%.

The nonsmooth appearance of the relations in Figure 1b can be explained by the finite resolution of the computational mesh; as the extent of a real cavity cannot always coincide with nodes of the mesh, the resulting calculation of drag and slip velocity is affected. We expect this numerical artifact to disappear with mesh refinement as in Gagliardini et al. (2007).

3.2. Obstacles With Different Widths and Spacings

To investigate the effect of lateral variations in bed topography on the sliding relation, we retain the along-flow sinusoidal geometry of the bed but introduce a function to vary the transverse width and spacing of bed obstacles. This function is

$$h(y; y_c, \epsilon_1, \epsilon_2, w) = 0.5 \left[\tanh \left(\frac{y - (y_c + w/2)}{\epsilon_1} \right) - \tanh \left(\frac{y - (y_c - w/2)}{\epsilon_2} \right) \right], \quad (9)$$

where y_c and w are the center y coordinate and transverse width, respectively, and ϵ_1 and ϵ_2 are smoothing factors. We let the center of the obstacles be $y_c = 2.5$ m and $y_c = 7.5$ m with symmetrical smoothing $\epsilon_1 = \epsilon_2 = 0.2$, resulting in two offset flow-parallel lines of obstacles, similar to the cross-sinusoidal bed (Figures 2a and S3):

$$z_b(x, y) = 0.8(\cos(2\pi x/10)h(y; y_c = 2.5) + \cos(2\pi x/10 - \pi)h(y; y_c = 7.5)).$$

We consider multiple obstacle widths (i.e., $w = 4.4$ m, 4.0 m, 3.6 m, 3.2 m, 2.8 m, and 2.4 m) to calculate an ensemble of sliding relations (Figure 2b) for the same range of top boundary velocities ($u_e = 0.2\text{--}32$ m/year).

For smaller transverse widths of obstacles and larger obstacle spacings, the extent of rate weakening becomes more pronounced (Figure 2b). From the widest to narrowest obstacles considered, peak drags decrease 50%, and ranges of sliding velocity with rate strengthening decrease 79%.

3.3. Steeply Inclined Stoss Sides

Having considered idealized 3-D geometries that result in rate-weakening drag, we now consider whether adding more complexity to the bed can affect this result. Constraints on Iken's bound (equation (2)) motivate us, in particular, to consider the effects of locally steep adverse slopes of 3-D bedforms. To characterize the along-flow topography, we use equation (9) with analogous along-flow parameters but with different smoothing factors (i.e., we use $h(x; \epsilon_1 = 0.3, \epsilon_2 = 2.0)$) to create 5-m-long, asymmetric obstacles (Figures 3 and S3) with steep stoss surfaces ($m_{\max} = 1.63$, relative to $m_{\max} = 0.50$ for the along-flow sinusoidal case).

The effect of steep stoss surfaces is that drag increases monotonically with the scaled sliding velocity over a range of sliding velocity that is 35 times higher than for the case of bedforms with smaller adverse slopes. Up to the transitional velocity at which rate weakening ensues, the relation is in conceptual agreement with the form of sliding relations that neglect cavity formation (equation (1)) and in contrast to the rate-weakening drag for an otherwise identical bed with sinusoidal obstacles (Figure 3). However, the peak drag for these narrow asymmetric obstacles is only 16% of Iken's bound computed in the absence of transverse topography.

4. Discussion

Interpreting the effect of local bed morphology on sliding relations requires considering the factors that control cavity size: the sliding velocity, which moves ice away from lee surfaces thereby opening cavities, and the creep rate of ice toward the bed that closes cavities and increases with effective pressure and cavity size. The computed stresses, cavities, and drag/velocity relations (Figures 1–3) reflect when these two processes are exactly balanced, so that cavity size is steady. Steady sliding is the natural starting point for simulations with 3-D beds.

Extending the well-studied case of a 2-D sinusoidal bed to the cross-sinusoidal case (Figure 1a) shows that the degrees of rate weakening in the two cases, scaled to effective pressure, are similar (Figure 1b). Absolute (dimensional) drag, however, decreases less in the cross-sinusoidal case. This may be because growth of cavities above the size necessary for the peak drag is reduced by ice being able to creep both downward and laterally toward cavities, so their steady length is smaller, allowing more steeply inclined zones of ice-bed contact. The peak drag, however, scaled in the way as a friction coefficient, is 43% smaller than in the 2-D case. Relative to the 2-D case, in which steep stoss surfaces in contact with ice have lateral continuity, for the cross-sinusoidal bed, such areas are a much smaller fraction of the total bed area, so the integration of equation (5) yields a smaller along-flow basal shear stress. This would imply, for example, that the same peak shear stress condition for the 3-D and 2-D cases will be reached at much lower water pressure for the 3-D case.

The finding that as obstacles get narrower (Figure 2) the extent of rate-weakening drag is increased may seem counterintuitive, given that narrow obstacles might be expected to support smaller cavities. However, as obstacle width decreases, progressively wider corridors of flat topography support minimal drag between obstacles. Stresses are thus laterally transferred to the obstacle sides (Figure S4), causing larger cavities that restrict zones of ice-bed contact to higher, more gently sloping parts of stoss surfaces.

Bed obstacles with sufficiently steep stoss surfaces can prevent, over a wide range of scaled sliding velocity, the rate-weakening drag (Figure 3) otherwise illustrated by our calculations with 3-D beds. Compared to the 2-D infinite slope considered by Gagliardini et al. (2007), which causes a severe, step-like reduction in drag at the velocity at which the steepest part of the stoss slope is inundated, rate weakening for the 3-D bed is gradual. Cavities can grow in 3-D so that the steepest part of the adverse slope is gradually overtaken. Steep stoss surfaces like those considered here are commonly observed on glacier beds, particularly where near-vertical fractures in the bed strike subperpendicular to glacier flow and control bedrock erosion (Hooyer et al., 2012). Although results of theory for 2-D wavy beds indicate rate-weakening drag, theoreticians have tended to advocate, on heuristic grounds, drag relations that neglect it, such that drag increases asymptotically toward a maximum value (Fowler, 1987; Schoof, 2005). Our results with obstacles with steep

adverse slopes indicate that they can greatly increase the range of slip velocity (or range of effective pressure) over which such heuristic sliding relations are appropriate. This finding helps justify the slip relations of large-scale ice sheet models and landscape evolution models, in which the potential for rate-weakening drag is neglected.

5. Conclusions

These numerical simulations show that sliding relations for 3-D beds that include effects of cavities can be acutely sensitive to nuances of local bed topography. A cross-sinusoidal bed supports lower drag, scaled as a friction coefficient by dividing drag by effective pressure, than an analogous bed with only along-flow roughness. Increasingly narrow and widely spaced obstacles cause increasingly severe rate weakening, owing to larger cavities and associated less steeply inclined areas of ice-bed contact, while significantly decreasing the bed friction coefficient. Sufficiently steep stoss surfaces of periodic obstacles on the bed can greatly increase the slip velocity or decrease the effective pressure at which rate-weakening drag occurs, broadening the range over which heuristic, rate-strengthening sliding relations used in glacier models apply. Bracketing the range of possible sliding behavior and the associated uncertainty of glacier flow-model predictions will require characterizing the morphological diversity of glacier beds and calculating sliding relations on that basis.

Acknowledgments

Contributions to this work by C. H., N. I., and L. Z. were supported by a grant from the U.S. National Science Foundation (EAR-1660972) to N. I. and L. Z. O. G. was supported by the French National Research Agency project SAUSSURE (ANR-18-CE01-0015-01). Functions specifying the bed topographies and numerical values for the variables used in the sliding relations are permanently archived at the Iowa State University Open Data repository (<https://doi.org/10.25380/iastate.11354111>). We appreciate the constructive comments by V. Tsai and two anonymous reviewers on an earlier version of the manuscript.

References

- Bindschadler, R. A., Nowicki, S., Abe-Ouchi, A., Aschwanden, A., Choi, H., Fastook, J., et al. (2013). Ice-sheet model sensitivities to environmental forcing and their use in projecting future sea level (the SeaRISE project). *Journal of Glaciology*, 59, 195–224. <https://doi.org/10.3189/2013JoG12J125>
- Brinkerhoff, D. J., & Johnson, J. V. (2013). Data assimilation and prognostic whole ice sheet modelling with the variationally derived, higher order, open source, and fully parallel ice sheet model VarGlaS. *The Cryosphere*, 7(4), 1161–1184. <https://doi.org/10.5194/tc-7-1161-2013>
- Brondex, J., Gagliardini, O., Gillet-Chaulet, F., & Durand, G. (2017). Sensitivity of grounding line dynamics to the choice of the friction law. *Journal of Glaciology*, 63(241), 854–866. <https://doi.org/10.1017/jog.2017.51>
- Budd, W. F., Keage, P. L., & Blundy, N. A. (1979). Empirical studies of ice sliding. *Journal of Glaciology*, 23(89), 157–170. <https://doi.org/10.3198/1979JoG23-89-157-170>
- Cuffey, K. M., & Paterson, W. S. B. (2010). *The physics of glaciers*. Amsterdam: Academic Press.
- Egholm, D., Nielsen, S., Pedersen, V., & Lesemann, J.-E. (2009). Glacial effects limiting mountain height. *Nature*, 460, 884–887. <https://doi.org/10.1038/nature08263>
- Fowler, A. C. (1981). A theoretical treatment of the sliding of glaciers in the absence of cavitation. *Philosophical Transactions of the Royal Society of London. Series A, Mathematical and Physical Sciences*, 298(1445), 637–681. <https://doi.org/10.1098/rsta.1981.0003>
- Fowler, A. C. (1986). A sliding law for glaciers of constant viscosity in the presence of subglacial cavitation. *Proceedings of the Royal Society of London Series A*, 407, 147–170. <https://doi.org/10.1098/rspa.1986.0090>
- Fowler, A. C. (1987). Sliding with cavity formation. *Journal of Glaciology*, 33(115), 255–267. <https://doi.org/10.3198/1987JoG33-115-255-267>
- Gagliardini, O., Cohen, D., Råback, P., & Zwinger, T. (2007). Finite-element modeling of subglacial cavities and related friction law. *Journal of Geophysical Research*, 112, F02027. <https://doi.org/10.1029/2006JE000576>
- Gagliardini, O., Zwinger, T., Gillet-Chaulet, F., Durand, G., Favier, L., de Fleurian, B., et al. (2013). Capabilities and performance of Elmer/Ice, a new generation ice-sheet model. *Geoscientific Model Development*, 6, 1299–1318.
- Geuzaine, C., & Remacle, J.-F. (2009). Gmsh: A 3-D finite element mesh generator with built-in pre- and post-processing facilities. *International Journal for Numerical Methods in Engineering*, 79(11), 1309–1331. <https://doi.org/10.1002/nme.2579>
- Gillet-Chaulet, F., Durand, G., Gagliardini, O., Mosbeux, C., Mouginot, J., Remy, F., & Ritz, C. (2016). Assimilation of surface velocities acquired between 1996 and 2010 to constrain the form of the basal friction law under Pine Island Glacier. *Geophysical Research Letters*, 43, 10,311–10,321. <https://doi.org/10.1002/2016GL069937>
- Glen, J. W. (1955). The creep of polycrystalline ice. *Proceedings of the Royal Society of London. Series A. Mathematical and Physical Sciences*, 228(1175), 519–538. <https://doi.org/10.1098/rspa.1955.0066>
- Gudmundsson, G. H. (1997). Basal-flow characteristics of a non-linear flow sliding frictionless over strongly undulating bedrock. *Journal of Glaciology*, 43(143), 80–89. <https://doi.org/10.3189/S0022143000002835>
- Hallet, B. (1979). A theoretical model of glacial abrasion. *Journal of Glaciology*, 23(89), 39–50. <https://doi.org/10.3189/S0022143000029725>
- Hallet, B. (1996). Glacial quarrying: A simple theoretical model. *Annals of Glaciology*, 22, 1–8. <https://doi.org/10.3189/1996AoG22-1-1-8>
- Hallet, B., & Anderson, R. (1980). Detailed glacial geomorphology of a proglacial bedrock area at Castleguard Glacier, Alberta, Canada. *Zeitschrift für Gletscherkunde und Glazialgeologie*, 16, 171–184.
- Harrison, W. D., Osipova, G. B., Nosenko, G. A., Espizua, L., Käab, A., Fischer, L., & Lai, A. W. (2015). Chapter 13—Glacier surges. In J. F. Shroder, W. Haeberli, & C. Whiteman (Eds.), *Snow and ice-related hazards, risks and disasters* (pp. 437–485). Boston. <https://doi.org/10.1016/B978-0-12-394849-6.00013-5>
- Herman, F., Beaud, F., Champagnac, J.-D., Lemieux, J.-M., & Sternai, P. (2011). Glacial hydrology and erosion patterns: A mechanism for carving glacial valleys. *Earth and Planetary Science Letters*, 310(3-4), 498–508.
- Hooke, R. L. (2005). *Principles of glacier mechanics* (2nd ed.). Cambridge: Cambridge University Press. <https://doi.org/10.1017/CBO9780511614231>
- Hooyer, T. S., Cohen, D., & Iverson, N. R. (2012). Control of glacial quarrying by bedrock joints. *Geomorphology*, 91–101. <https://doi.org/10.1016/j.geomorph.2012.02.012>
- Iken, A. (1981). The effect of the subglacial water pressure on the sliding velocity of a glacier in an idealized numerical model. *Journal of Glaciology*, 27(97), 407–421. <https://doi.org/10.3198/1981JoG27-97-407-421>

- Iken, A., & Bindschadler, R. A. (1986). Combined measurements of subglacial water pressure and surface velocity of Findelengletscher, Switzerland: Conclusions about drainage system and sliding mechanism. *Journal of Glaciology*, 32(110), 101–119. <https://doi.org/10.3198/1986JoG32-110-101-119>
- Jansson, P. (1995). Water pressure and basal sliding on Storglaciären, northern Sweden. *Journal of Glaciology*, 41(138), 232–240. <https://doi.org/10.3198/1995JoG41-138-232-240>
- Joughin, I., Smith, B. E., & Schoof, C. G. (2019). Regularized Coulomb friction laws for ice sheet sliding: Application to Pine Island Glacier, Antarctica. *Geophysical Research Letters*, 46, 4764–4771. <https://doi.org/10.1029/2019GL082526>
- Kamb, B. (1970). Sliding motion of glaciers: Theory and observation. *Reviews of Geophysics*, 8(4), 673–728. <https://doi.org/10.1029/RG008i004p00673>
- Kamb, B. (1987). Glacier surge mechanism based on linked cavity configuration of the basal water conduit system. *Journal of Geophysical Research*, 92(B9), 9083–9100. <https://doi.org/10.1029/JB092iB09p09083>
- Koellner, S., Parizek, B. R., Alley, R. B., Muto, A., & Holschuh, N. (2019). The impact of spatially-variable basal properties on outlet glacier flow. *Earth and Planetary Science Letters*, 515, 200–208. <https://doi.org/10.1016/j.epsl.2019.03.026>
- Larour, E., Seroussi, H., Morlighem, M., & Rignot, E. (2012). Continental scale, high order, high spatial resolution, ice sheet modeling using the Ice Sheet System Model (ISSM). *Journal of Geophysical Research*, 117, F01022. <https://doi.org/10.1029/2011JF002140>
- Lliboutry, L. (1968). General theory of subglacial cavitation and sliding of temperate glaciers. *Journal of Glaciology*, 7(49), 21–58. <https://doi.org/10.3198/1968JoG7-49-21-58>
- Lylly, M., Ruokolainen, J., & Järvinen, E. (1999). ELMER-a finite element solver for multiphysics. *CSC-Report on Scientific Computing*, 2000, 156–159.
- Maier, N., Humphrey, N., Harper, J., & Meierbach, T. (2019). Sliding dominates slow-flowing margin regions, Greenland Ice Sheet. *Science Advances*, 5(7), eaaw5406. <https://doi.org/10.1126/sciadv.aaw5406>
- Morlighem, M., Rignot, E., Seroussi, H., Larour, E., Ben Dhia, H., & Aubry, D. (2010). Spatial patterns of basal drag inferred using control methods from a full-Stokes and simpler models for Pine Island Glacier, West Antarctica. *Geophysical Research Letters*, 37, L14502. <https://doi.org/10.1029/2010GL043853>
- Muto, A., Anandakrishnan, S., Alley, R. B., Horgan, H. J., Parizek, B. R., Koellner, S., et al. (2019). Relating bed character and subglacial morphology using seismic data from Thwaites Glacier, West Antarctica. *Earth and Planetary Science Letters*, 507, 199–206. <https://doi.org/10.1016/j.epsl.2018.12.008>
- Nye, J. F. (1969). A calculation on the sliding of ice over a wavy surface using a Newtonian viscous approximation. *Proceedings of the Royal Society of London. A. Mathematical and Physical Sciences*, 311(1506), 445–467. <https://doi.org/10.1098/rspa.1969.0127>
- Pedersen, V., & Egholm, D. (2013). Glaciations in response to climate variations preconditioned by evolving topography. *Nature*, 493, 206–210. <https://doi.org/10.1038/nature11786>
- Pelletier, J. D. (2008). Glacial erosion and mountain building. *Geology*, 36(7), 591–592. <https://doi.org/10.1130/focus072008.1>
- Råback, P., Malinen, M., Ruokolainen, J., Pursula, A., & Zwinger, T. (2019). Elmer models manual [computer software manual]. <http://www.nic.funet.fi/pub/sci/physics/elmer/doc/ElmerModelsManual.pdf> [Accessed:2019-08-03]. CSC-ITCenterforScience
- Ritz, C., Edwards, T., Durand, G., Payne, A., Peyaud, V., & Hindmarsh, R. (2015). Potential sea-level rise from Antarctic ice-sheet instability constrained by observations. *Nature*, 528, 115–118. <https://doi.org/10.1038/nature16147>
- Schoof, C. (2005). The effect of cavitation on glacier sliding. *Proceedings of the Royal Society of London. A. Mathematical and Physical Sciences*, 461(2055), 609–627. <https://doi.org/10.1098/rspa.2004.1350>
- Thøgersen, K., Gilbert, A., Schuler, T., & Maithe-Sørensen, A. (2019). Rate-and-state friction explains glacier surge propagation. *Nature Communications*, 10, 2823. <https://doi.org/10.1038/s41467-019-10506-4>
- Torres, M. A., Moosdorf, N., Hartmann, J., Adkins, J. F., & West, A. J. (2017). Glacial weathering, sulfide oxidation, and global carbon cycle feedbacks. *Proceedings of the National Academy of Sciences*, 114(33), 8716–8721. <https://doi.org/10.1073/pnas.1702953114>
- Tsai, V. C., Stewart, A. L., & Thompson, A. F. (2015). Marine ice-sheet profiles and stability under Coulomb basal conditions. *Journal of Glaciology*, 61(226), 205–215. <https://doi.org/10.3189/2015JoG14J221>
- Ugelvig, S. V., & Egholm, D. L. (2018). The influence of basal-ice debris on patterns and rates of glacial erosion. *Earth and Planetary Science Letters*, 490, 110–121. <https://doi.org/10.1016/j.epsl.2018.03.022>
- Walder, J., & Hallet, B. (1979). Geometry of former subglacial water channels and cavities. *Journal of Glaciology*, 23(89), 335–346. <https://doi.org/10.3189/S0022143000029944>
- Weertman, J. (1957). On the sliding of glaciers. *Journal of Glaciology*, 3(21), 33–38. <https://doi.org/10.3198/1957JoG3-21-33-38>
- Zoet, L. K., & Iverson, N. R. (2015). Experimental determination of a double-valued drag relationship for glacier sliding. *Journal of Glaciology*, 61(225), 1–7. <https://doi.org/10.3189/2015JoG14J174>
- Zoet, L. K., & Iverson, N. R. (2016). Rate-weakening drag during glacier sliding. *Journal of Geophysical Research: Earth Surface*, 121, 1206–1217. <https://doi.org/10.1002/2016JF003909>

References From the Supporting Information

- Babuška, I. (1973). The finite element method with Lagrangian multipliers. *Numerische Mathematik*, 20(3), 179–192. <https://doi.org/10.1007/BF01436561>
- Brezzi, F. (1974). On the existence, uniqueness and approximation of saddle-point problems arising from Lagrangian multipliers. *ESAIM: Mathematical Modelling and Numerical Analysis - Modélisation Mathématique et Analyse Numérique*, 8(R2), 129–151. <https://doi.org/10.1051/m2an/197408R201291>
- Franca, L. P., & Frey, S. L. (1992). Stabilized finite element methods: II. The incompressible Navier-Stokes equations. *Computer Methods in Applied Mechanics and Engineering*, 99(2), 209–233. [https://doi.org/10.1016/0045-7825\(92\)90041-H](https://doi.org/10.1016/0045-7825(92)90041-H)
- John, V. (2002). Slip with friction and penetration with resistance boundary conditions for the Navier-Stokes equations - numerical tests and aspects of the implementation. *Journal of Computational and Applied Mathematics*, 147, 287–300. [https://doi.org/10.1016/S0377-0427\(02\)00437-5](https://doi.org/10.1016/S0377-0427(02)00437-5)